THE IMPORTANCE OF BEING ON TIME: DELAYED NEUROFEEDBACK IMPEDES TRAINING OF THE PARIETAL ALPHA-BAND POWER

A PREPRINT

Anastasiia Belinskaia
Center for Bioelectric Interfaces
Higher School of Economics
Moscow, Russia, 101000

Nikolai Smetanin
Center for Bioelectric Interfaces
Higher School of Economics
Moscow, Russia, 101000

Mikhail Lebedev
Center for Bioelectric Interfaces
Higher School of Economics
Moscow, Russia, 101000

Alexei Ossadtchi*
Center for Bioelectric Interfaces
Higher School of Economics
Moscow, Russia, 101000
ossadtchi@gmail.com

July 27, 2020

Abstract

The therapeutic effects of neurofeedback (NFB) remain controversial. Here we show that NFB latency affects the ability of subjects to increase their parietal electroencephalographic alpha activity. Visual NFB was delivered either as soon as EEG was processed, or with a 250 or 500-ms added delay. After the training, a sustained increase in alpha average magnitude was observed only for the shortest latency tested. During the NFB sessions, learning profiles varied with latency, as shown with the adaptive Neyman test. The steepest growth of alpha magnitude was observed also for the shortest latency. For all latencies, NFB affected only the alpha spindle occurrence rate, not their duration or amplitude. The effectiveness of NFB only at the short-latency could explain the failures of some of the previous studies, where this parameter was neither controlled nor documented. Clinical practitioners and manufacturers of NFB equipment should include latency in their specifications, and enable short-latency operations.

Introduction

In this study, we implemented a neurofeedback (NFB) task, where participants self-controlled their parietal electroencephalographic (EEG) rhythms, and investigated how setting NFB latency to different values affected the EEG patterns.

NFB is a closed-loop paradigm, where subjects are presented with an indicator of their own brain activity, which they learn to change in a certain desired way [25], [26], [53], [55], [60]. In a typical NFB experiment, neural activity is recorded, converted into features of interest, processed to generate an output signal, and delivered to the subject as a sensory stimulus, typically visual or auditory. Training with NFB results in plastic changes in the neural circuits involved. This type of learning fits the definition of operant conditioning, where the behavioral responses are derived directly from neural activity, and indicators of successful performance presenting to the subjects serve as rewards that reinforce the wanted behavior [53]. Historically, the first implementations of NFB were based on EEG recordings [25], [26], followed by more recent demonstrations based on such recording methods as magnetoencephalography (MEG) [38], [4], functional magnetic resonance imaging (fMRI) [59], [65], functional near-infrared spectroscopy (fNIRS) [28], and depth electrodes [68].

Practical interest to NFB approach is driven by the expectation that it could become a powerful therapy that improves brain processing in subjects suffering from neurological disorders [60]. Since, at least theoretically, NFB could target neural circuits very specifically, this method could supplement or even replace the traditional pharmacological [63], [3], [70], [31] and cognitive-enhancement [69], [10] therapies. However, despite the high expectations and numerous studies on NFB-based therapies, this approach remains controversial because of the high variability of its outcomes and the lack of improvement in a considerable number of cases [2], [60]. The difficulties in the development of efficient NFB-based therapies are rooted in the insufficient understanding of the physiological effects of NFB [24], issues related to ergonomics, and problems in signal processing [22].

Here we looked into the issue that has not been sufficiently addressed by previous research on NFB: the proper setting of NFB latency, that is the time interval from the occurrence of a neural activity till the delivery of the feedback of that activity to the subject. NFB latency specifies the reinforcement schedule [53] and as such it should significantly affect the outcome of operant conditioning [49], [44].

Temporal specificity is of essential importance for neural processing [23], and feedback latency plays a pivotal role in a range of closed-loop systems, including nonlinear dynamical systems [66] and biological systems with a delay [33], [6]. Moreover, human psychophysics studies have demonstrated that feedback latency significantly influences sensory, motor, and cognitive processing. Thus, visual perception and performance are impaired when human subjects observe images on the displays with lags and slow frame rate [9]. Additionally, delaying visual feedback diminishes the accuracy of drawing [17], and accuracy of slow but not fast reaching movements toward a target is impaired if the light is suddenly turned off [27]. In a virtual environment, feedback latency affects the sense of presence, particularly when the environment is stressful [35]. Furthermore, the sense of agency, that is the perception of being in control of own movements, deteriorates with an increase of the visual feedback delay [16]. Similarly, the telepresence level, when using a surgical robot, decreases with increasing feedback delay [50].

The effects of feedback latency have been recognized in the literature on NFB and brain-computer interfaces (BCIs). Oblak et al. [37] simulated fMRI signals in visual cortex and had human subjects develop cognitive strategies to utilize NFB produced from the simulated data. They observed a better performance for continuous NFB than for intermittent NFB. Additionally, NFB delay significantly affected the performance with continuous NFB. Furthermore, they developed a computational model of automatic NFB learning. This modeling showed that when NFB was blurred and arrived with a delay, the performance was better with intermittent feedback compared to continuous feedback. The authors suggested that NFB settings should be optimized to match the experimental paradigm and learning mechanism (cognitive versus automatic). Evans et al. [14] implemented a motor imagery-based BCI where the control signal was derived from sensorimotor mu or beta rhythms. They showed that introduction of a feedback delay resulted in a reduced sense of agency, that is subjects did not perceive the BCI output as the result of their voluntary intentions.

In the present study, we implemented a NFB derived from the parietal alpha rhythm and for the first time systematically investigated the effect of NFB latency on the changes in EEG patterns. There is a vast literature on brain rhythms [7] and on NFB paradigms for controlling the rhythms in different brain areas [69], [18], [58]. Brain rhythms typically wax and wane, which makes it important to understand their temporal structure when setting NFB parameters. In addition to the temporal dimension, space [32] and frequency [20], [62] are the dimensions that carry specific information that could be utilized to generate NFB. The following reasons motivated our choice of alpha rhythm as the source of NFB. First, alpha rhythm is one of the most prominent and most responsive to training brain rhythms [36], [1], [12], [19], [21], [61]. According to the existing literature and our own results [41], parietal alpha rhythm easy to isolate (in contrast to the sensorimotor rhythm, for example) and is easy to train with NFB practically in all subjects. Moreover, NFB that is based on the parietal alpha rhythms has been suggested as the approach to gaining a range of functional improvements, including improvements in cognition [61], [1], [19], attention [4], [39], [40], [8], working memory [11], [67], mood [42], [13], [43], and relaxation [5].

NFB latency results from the signal processing pipelines that comprises several stages, see Figure 1 A. The overall latency is the time from the occurrence of a neuronal event being tracked till the instance when the subject receives an NFB replica of this event. This time includes a data collection interval (tens of milliseconds), interval of filtering and instantaneous power estimation (hundreds of milliseconds), and feedback generation interval (tens of milliseconds). In the currently used NFB systems, latency falls within the range from 300 to 1000 ms. This duration can be decreased by means of optimizing data acquisition and signal processing steps. To this end, we recently developed NFB-Lab software [57], where we implement a novel causal complex-valued finite impulse response (cFIR) approach for simultaneous narrow-band filtering and extracting the instantaneous power of an EEG rhythm [56]. This method allowed us to achieve high accuracy of narrow-band power estimation with the lag as short as 100 ms. In this implementation communication with the EEG recording system was enabled by the Lab Streaming Layer protocol [29], followed by prefiltering, and visual stimulus delivery which all together incurred approximately 144-ms average lag. Thus, the mean overall latency was 244 ms in our system. We refer to this delay as system's base latency.

In this study we employed the NFB Lab software and the cFIR approach, to examine NFB performance for several overall latency values in 244–744 ms range. We found that the increased delay adversely affected both the dynamics of training and the sustainability of the incurred plastic changes.

Methods

Participants and settings

Forty healthy right-handed subjects (13 males and 27 females; aged 24.58 +- 5.3 years, mean +- SD) participated in the experiments. The study was conducted in accordance with the ethical standards of the 1964 Declaration of Helsinki. All participants provided written informed consent prior to the experiments. The ethics research committee of the National Research University, The Higher School of Economics approved the experimental protocol of this study.

The NFB signal was derived from the P4 channel (corresponding to the right parietal region). An alpha envelope was visualized as a circle with a pulsating outline. The subjects had to smooth that outline by increasing their P4 alpha-band power.

All participants were given the same instruction. They were instructed to refrain from using any conscious strategy. This assured that learning to control the parietal alpha rhythm was automatic [30], which was the mode where the latency of a continuous NFB should hypothetically have a stronger effect on the performance [37].

Subjects sat in a comfortable chair at a distance of 80 cm from an LCD monitor with a 24-cm diagonal and a 60-Hz refresh rate. These settings remained constant throughout the entire experiment.

EEG signals were recorded using 32 AgCl electrodes placed according to the 10-20-system. Each EEG channel was sampled at 500 Hz using an NVX-136 amplifier (Medical Computer Systems Ltd) and bandpass-filtered in the 0,5 - 70 Hz band. These preprocessing filters incurred an overall delay of no more than 10 milliseconds for the bandwidth of interest (8–12 Hz). Digital common ear reference was derived from the electrodes placed on both ears. The impedance for each electrode was kept below 10 KOhm.

Experimental protocol and measurements

The participants were split into four equal groups, each with different NFB settings: (1) NFB with no delay added to the system's base latency of 244 ms (FB0), (2) NFB with a 250-ms delay added (FB250), (3) NFB with a 500-ms delay added (FB500), (4) mock NFB where the feedback was generated from EEG data taken from a different participant (FBmock). Due to a technical problem associated with an intermittently suspended EEG-software communication, we had to exclude the records of 5 subjects (2 from FB0 group, 2 from FBMock group, and 1 from FB500 group) from the final analysis. When choosing statistical methods, we took into consideration these unequal sample sizes. The details of the statistical analysis can be found in the section Results and Appendix: Comparing learning curves.

The experimental sequence is shown in Figure 1 B. Prior to NFB sessions, we collected resting-state EEG data and used them to set the spatial filters for the suppression of eye-movement artifacts and to determine the frequency of alpha rhythm in individual subjects (for more details, see EEG data processing). Next, just prior to NFB training we recorded a 2-min Baseline with eyes open. Then, the actual NFB training started that comprised fifteen two-minute blocks with NFB control separated by 15-s resting periods. Immediately following the NFB training we recorded the post-training 2-minute Baseline.

Composition of subject groups

When composing the subject groups, we had to deal with the differences in alpha rhythm patterns in individual subjects. These individual features were evident from the resting-state data. Notably, resting-state alpha amplitude is predictive of the subject's subsequent improvement in NFB control with training [64]. This effect could contribute to the heterogeneity of subjects across groups (FB0, FB250, FB500, FBmock) in our study. For instance, a subject with a weak alpha rhythm would not be able to improve in NFB control in any condition, but his/her assignment to a particular group could produce a false group-related result. To control for this effect, we implemented a stratified sampling procedure [47], [45], [51], [48] that equalized resting-state alpha amplitude across groups. We measured signal to noise ratio (SNR) for the alpha amplitude while participants rested with open eyes, and categorized them as having high alpha (SNR >4,4; Mean (2,89) +SD (1,51)), low alpha (SNR <1,38; Mean (2,89) - SD(1,51)), or medium alpha (1,38 <SNR <4,4). Each subject was assigned to a NFB group with the procedure where the NFB group was randomly selected, but if the SNR category (high, low or medium alpha) was already filled for that group with the entries from the other subjects, random selection repeated [47] (for more details, see "Signal to noise ratio" section

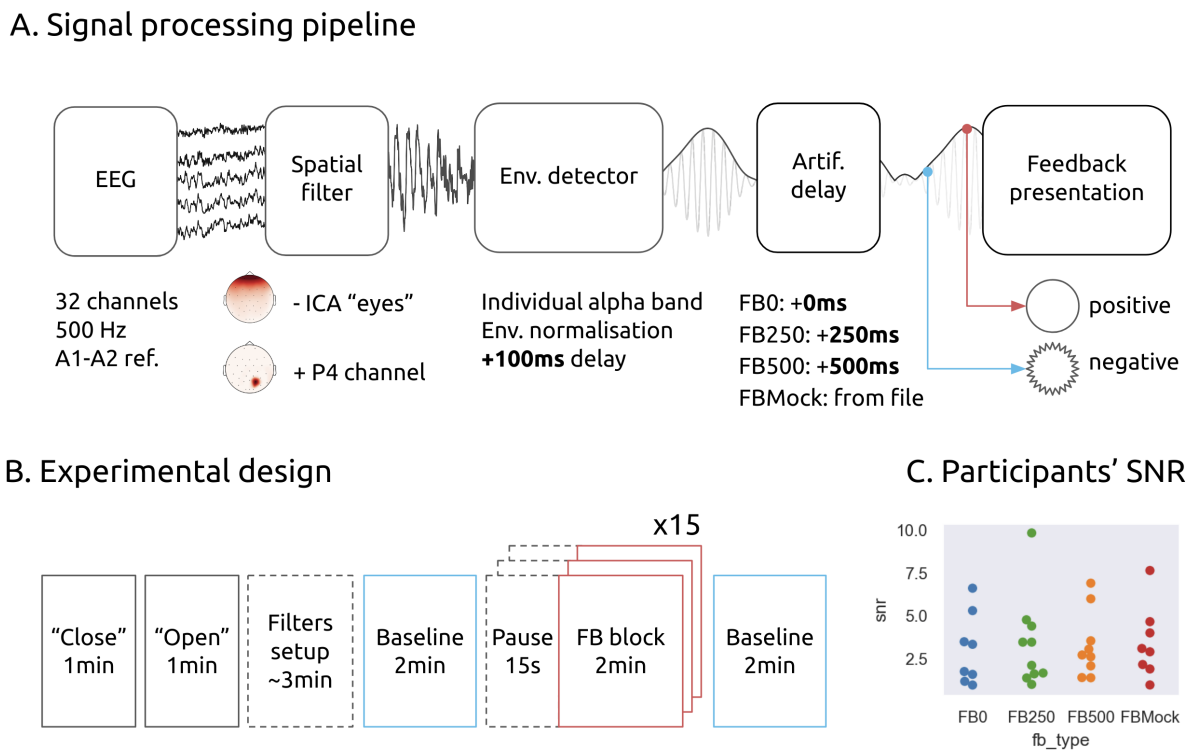

Figure 1: Schematics of signal processing and experimental settings. A: Signal processing pipeline, where multichannel EEG signals are processed by a spatial filter to remove artifacts, converted into a narrow-band signal, time shifted with an artificial delay, and converted into a visual feedback. B: Experimental design, where resting-state EEG activity is recorded first, followed by NFB sessions. In the end another baseline is recorded. C: Signal to noise ratio of alpha rhythm across NFB groups. Datapoints represent SNR value for each subject.

below). Wilcoxon rank-sum test showed no statistical difference between the SNR across the four experimental groups (Figure 1 C).

EEG data processing

Independent component analysis

As shown in Figure 1 B, the experiments started with the recording where a subject first looked at the fixation cross for one minute and then closed the eyes for one more minute. We then used these data to build a spatial filter based on the independent component analysis (ICA) to remove the artifacts caused by eye movements and blinking. This approach decomposed the EEG signals into independent components, including the ones containing the artifacts. Ocular artifact components were detected as those with the largest value of mutual information of their time-series and the signals in Fp1 and Fp2 channels, which are closest to the eyes. A spatial filter matrix was then constructed for the subsequent online application during the NFB sessions.

Individualized bandpass filter

Bandpass filters for extracting alpha activity were built separately for each individual. The signal was taken from channel P4. To detect alpha activity, we started with the frequency range 8 to 12 Hz, and then adjusted the range and filter parameters for each individual subject. We determined the central frequency F_c of the rhythm by visual inspection and then set the range relative to the central frequency as $[F_c - 2, F_c + 2]$. With this method, the selected target signal frequency range accurately reflected the individual subject alpha rhythm properties.

Signal to noise ratio

The SNR was calculated before the main session from the two-minute baseline as the ratio of the average power spectral density (PSD) magnitude within the individually determined target frequency range $[F_c - 2, F_c + 2]$ to the mean PSD magnitude within the two flanker sub-bands $[F_c - 4, F_c - 2)$ and $(F_c + 2, F_c + 4]$. The participants with SNR less or equal to 1 were not included into the pool of subjects. The participants with SNR greater than 1 were assigned to one of the experimental groups with a stratified sampling procedure (see "Composition of subject group" section above).

Envelope extraction

Alpha-rhythm envelope was extracted with the cFIR approach [56] (Figure 2 A). In this method, the raw EEG signal is transformed into a narrowband analytic signal, a complex-valued function whose absolute value corresponds to an instantaneous amplitude(or envelope) of the rhythm. The cFIR method allows us to explicitly define NFB latency and obtain a more accurate envelope estimate for a specified latency compared to the other approaches frequently used for quantification of narrowband components in the EEG data, [56]. This speed-accuracy trade-off can be appreciated from the accuracy vs. processing delay curves presented in Figure 2 B for the cFIR and the commonly used approach based on narrow-band filtering followed by signal rectification. In the present study, we set the cFIR delay parameter to 100 ms (the point marked by a cross in Figure 2 B). This setting corresponds to the correlation coefficient of 0.85 +- 0.1 between the actual and the on-line reconstructed envelopes.

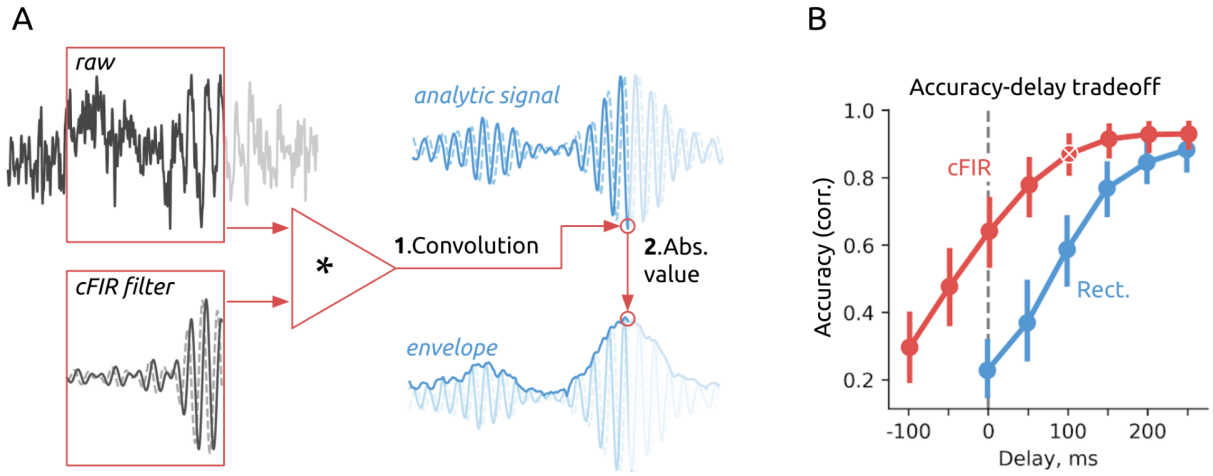

Figure 2: Schematics of envelope extraction. A: Graphical illustration of the cFIR method, where the envelope is obtained from the optimally-filtered complex-valued analytic signal. B: Speed-accuracy curve for envelope extraction with cFIR (red) and Rect (blue) methods. cFIR outperforms Rect for all latency values. The cFIR setting used in this study (latency of 100 ms) is designated by the cross.

Latency measurement

To monitor the system's total latency in accordance with the recommendations of the CRED-nf checklist [46], we used a direct latency measurement aided with a photosensor attached to the corner of the screen [57]. Figure 3 A explains this method for syncing the "brain time" (top), that is the actual time of the occurrence of neuronal events, and the "PC time", that is the time when these neuronal events are registered by the computer.

EEG signals are sampled by an EEGgraph and sent to the PC, where they are timestamped with an EEG to PC transmission delay. The EEG data are processed and converted into a feedback stimulus that is then presented on the screen. The time of the screen event is detected by the photo-sensor whose output is fed to one of the EEGgraph channels and transmitted back to the computer with the same delay as for the EEG to PC transfer. Therefore, the lag between the neural event (in our case, instantaneous alpha amplitude extracted from EEG with zero latency in an offline analysis) and the corresponding photosensor event is measured in reference to the PC time axis: it corresponded to the overall NFB latency.

We implemented this method by dedicating a small square in the upper-right screen corner to the photosensor signal. The square brightness corresponded to the NFB signal presented on the main portion of the screen, and the square itself was covered by the photosensor and therefore invisible to the participants. The square brightness, measured by the photosensor, was fed to an auxiliary channel of the EEG device and recorded together with the EEG data. The overall latency was estimated by comparing the photosensor signal, $p(t)$, with the zero-latency NFB signal calculated offline, $y_0(t)$ (Figure 3B). The lag between these two signals was calculated as the timing of the peak in their cross-correlation function (Figure 3 C). With this approach, amplitude and time, (R_{max}, τ_{max}), of the cross-correlation peak were computed for the entire duration of the experiment and used as the measurements of NFB average accuracy and latency.

To test the effects of changing the overall latency we either used the nominal 244-ms latency (group FB0) or artificially added an extra delay of 250 ms (FB250) or 500 ms (FB500) to the 244-ms latency. This resulted into three NFB conditions (FB0, FB250 and FB500) where the feedback arrived to a subject with delays of 244, 494 and 744 ms following the corresponding neuronal event. Mock feedback was used as a control condition.

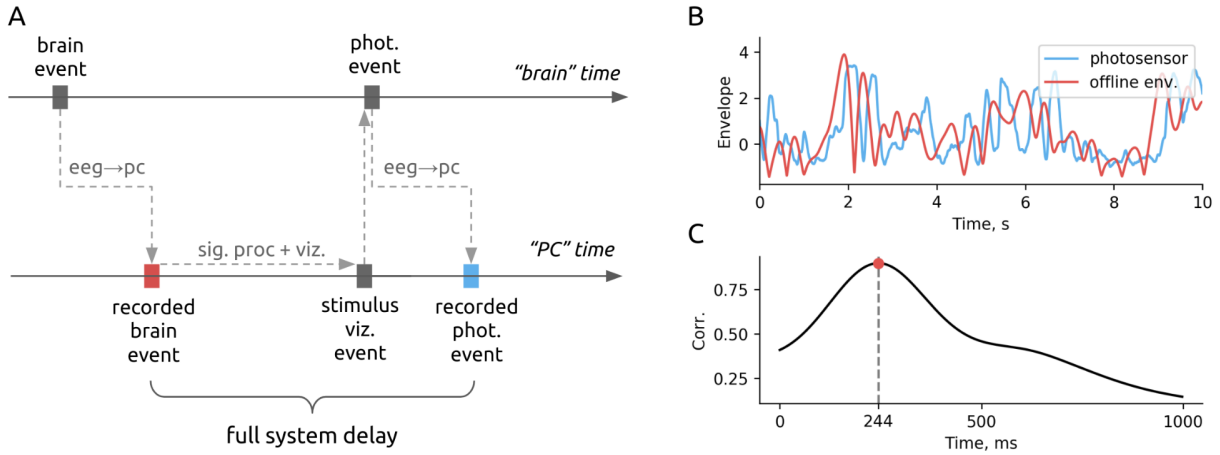

Figure 3: Schematics of the overall latency measurement. A: Syncing of the "brain time" (top) and "PC time" (bottom) using a photosensor. EEG signals (brain events) are registered by the computer with an EEG to PC lag. The computer sends a signal to the screen, which is measured by the photosensor and is then sent back to the computer through an auxiliary EEG channel with the same EEG to PC lag. The overall latency is the time from a brain event of interest (instantaneous alpha-band amplitude) till the corresponding photosensor event, with both measurements referred to the PC time axis. B: Zero-latency alpha amplitude, $y_0(t)$ (red) and the real-time NFB captured by the photosensor, $p(t)$ (blue). C: Crosscorrelation function betweeen $y_0(t)$ and $p(t)$ as a function of the time lag. The time of the crosscorrelation peak corresponds to the overall NFB latency.

Blinding

The experimental flow implied minimal interaction between the experimenter and the subject after the point when the group assignment was known as this happened using the described randomized stratification procedure past the moment when individual filters were setup. This means that briefing the subject, electrodes installation and recording of the first two 1-minute baselines occurred before the group assignment was generated by the computer and saved in the subject's folder.

When processing the data and generating the results we analyzed all data with a single script looping over all subjects from all four groups and applying the exactly identical processing pipeline. Then, the results of this stereotypical processing were grouped using the group assignment variable and the appropriate statistical comparison was also performed automatically. All data analysis scripts and the actual data are at `https://github.com/nikolaims/delayed_nfb`

Results

Effects of NFB latency on the P4 alpha rhythm magnitude

We first explored the changes in P4 alpha-band magnitude as a function of training block sequential index. Different shapes of these curves observed in different conditions reflect distinct training *dynamics*. Figure 4 shows the across-subject means of alpha-band magnitude computed for 15 training blocks; separate curves correspond to different NFB delays. In order to minimize inter-subject variability, each subject's data were normalized by dividing by the mean magnitude for all training blocks. Thus, if there is no training effect then across-subject mean values should exhibit a "flat" curve and concentrate around the constant level of 1. If NFB training results in alpha power increase then across-subject mean values should form a curve with an overall positive slope. Figure 4 shows that NFB training resulted in a noticeable gradual enhancement of the alpha rhythm magnitude for all tested latency values, and only a small enhancement occurred for the mock NFB.

We first quantified the changes in alpha magnitude using a classical linear regression model. The confidence intervals (CIs) for the linear correlation coefficient ρ are displayed on top of each panel in Figure 4. In the FBMock condition, the learning curve is noticeably flatter compared to the NFB conditions; iowever, in all four groups including FBMock, we found a significantly positive correlation between mean alpha rhythm magnitude within a block and block's sequential number. The 95 % confidence interval on ρ in FBMock condition does not overlap with the CIs for FB250 and FB500 conditions. The CIs for the linear correlation coefficient in FB0 and FBMock conditions overlap very slightly, primarily because of the prominent decline that occurred during the last three blocks in the FB0 condition.

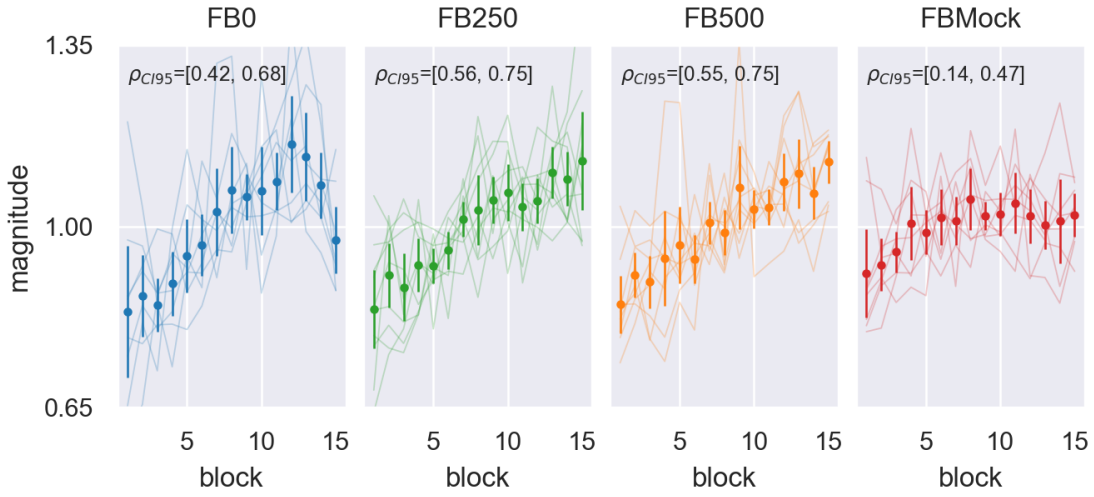

Figure 4: Learning curves reflecting changes in alpha-band magnitude across 15 experimental blocks. Thick lines correspond to the averaged individual subject curves (thin lines) within FB0, FB250, FB500, and FBMock conditions. Vertical bars correspond to two standard errors. The numbers on each plot correspond to the 95 % confidence interval for the linear correlation in each condition.

For a more detailed quantification of the learning curves, we performed the adaptive Neyman test (AN-test) proposed in [15]. This test considers the projections of the differences in t-statistics onto a set of orthogonal basis functions and assesses the significance of the projection coefficients. This approach takes into account the fact that the observed samples belong to a smooth curve. We applied this test but used Legendre orthogonal polynomials instead of Fourier basis as proposed in the original paper. This was done because the shapes of these individual basis functions allowed for a more parsimonious description of the typical NFB learning dynamics. The details of our implementation of this test can be found in Appendix: Comparing learning curves. Figure 5 A shows the results of applying the AN-test to pairwise comparison of P4 alpha magnitude learning curves observed in the four conditions.

As with a simple linear model, we found that all NFB conditions had training dynamics that was significantly different from that observed in FBMock condition. Interestingly, FB0 vs. FBMock t-statistics profile is characterized by the

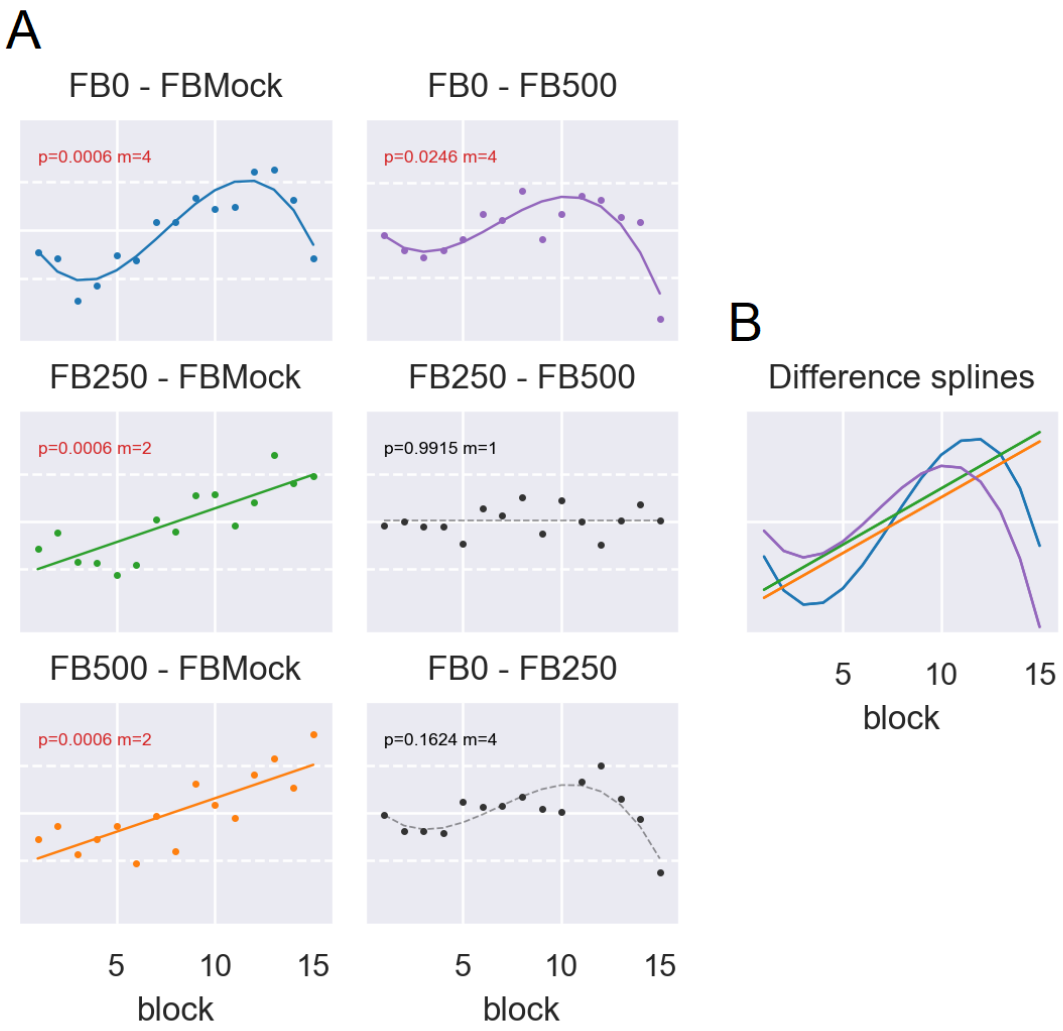

Figure 5: A detailed comparative pairwise analysis of alpha magnitude learning curves observed in four conditions. a) Pairwise t-statistics profiles. The corresponding FDR-corrected p-values and the number of used coefficients are shown in the top of each plot. b) Parametric differential profiles computed as linear combinations of significant polynomials for the four significant ($p < 0.05$) pairwise comparisons.

S-shape indicating the later onset of positive changes and earlier saturation with the subsequent decline. The test was also powerful enough to detect the difference in the learning curve shapes observed in FB0 and FB500 conditions. As evident from Figure 5 B, FB0 was characterized by a steeper learning curve compared to the ones observed in the other conditions (see FB0–FBMock and FB0–FB500 profiles). While the FB0 curve had the steepest rise, it saturated earlier compared to the other conditions and then declined.

As illustrated in Figure 1 B, we recorded 2 minutes of resting-state baseline EEG activity before and after NFB training. Figure 6 A shows the changes in the mean alpha power between the two baseline intervals for all subjects included in the four groups. Only FB0 condition shows statistical tendency for the growth in post-intervention alpha magnitude, $p = 0.022(0.0881)$, FDR corrected p-value is shown in brackets. The confidence interval for the mean paired difference in FB0 condition lies strictly in the positive range while the CIs for the other conditions include zero. No significant differences in feedback induced mean power gain was found via direct pairwise comparison of the three feedback conditions (FB0, FB250, FB500).

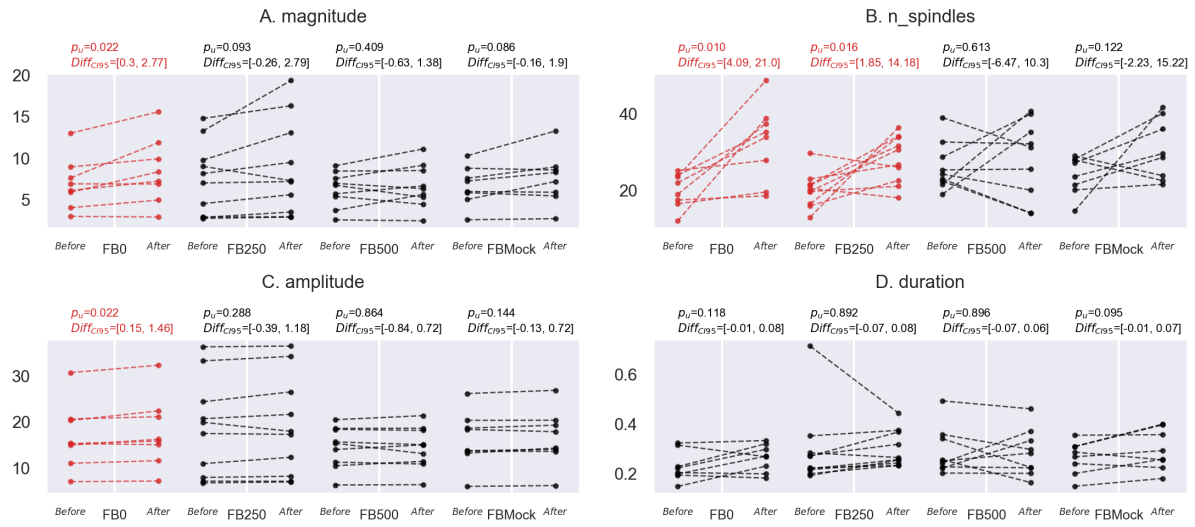

Figure 6: The pre-training and post-training baselines for A) alpha magnitude, B)burst incidence rate, C) burst amplitude and D) burst duration for four conditions of the study. The text above each column shows 95% confidence intervals on the mean paired difference and uncorrected p-values. FB0 condition shows a significant increase in post-training alpha magnitude, incidence rate and a small but consistent growth in the burst amplitude parameter.

Effects of NFB latency on the structure of P4 alpha activity

EEG rhythmic activity is non-stationary and consists of a succession of transient burst events. Changes in mean magnitude of alpha activity may be caused by variations in burst duration, burst amplitude, and the incidence rate of such bursts.

In our previous study with a relatively short and fixed NFB latency of 360 ms [41], we observed NFB-evoked changes in the incidence rate of alpha bursts but not in their amplitude and duration. Intriguingly, this observation that casts alpha-band bursts as structural units of alpha activity whose characteristics change during NFB-induced neural plasticity is consistent with the results of [54] where importance was highlighted of the discrete beta-spindles for motor control in several species.

Following the methodology of our previous study [41], for all four conditions, we analyzed the time course of burst characteristics, including incidence rate, amplitude, and duration. Alpha bursts extracted with simple thresholding from the envelope of the alpha-band filtered P4 time course, see Figure 7. By the analysis design, the characteristics of burst depend on the selected threshold. For example, if a high threshold value is used, only the most prominent episodes of alpha activity are qualified as bursts (Figure 7 A), while with a lower threshold value, the same bursts appear to have of a longer duration. Additionally, less prominent alpha episodes are also counted (Figure 7 B). Furthermore, with a low threshold, adjacent bursts could merge into a single one, thereby increasing the duration of bursts and reducing their count.

As a reasonable solution, we selected the threshold value that corresponded to the minimum mean mutual information (MI) between the three distinct pairs of morphological parameters: incidence rate vs. burst amplitude, incidence rate vs. burst duration, and burst amplitude vs. burst duration. This analysis leads us to select the threshold factor of $\mu = 2.5$. The actual threshold was then found by multiplying this factor by the median value of the time series.

To assess the effect of NFB training on the parameters of alpha bursts, we compared the three NFB groups (FB0, FB250, FB500) to FBMock group. The results of the AN-test for pairwise comparison for all rhythm characteristics changes (magnitude, number of bursts, amplitude, and duration) are shown in Figure 8 A. For all NFB conditions, the curves representing burst incidence rate are different from the corresponding curve for FBMock condition ($p < 0.02$, FDR corrected). As to the curves for alpha-spindle duration and amplitude no significant difference is present between the NFB and mock NFB conditions. This result replicates our previous observation [41] and extends it to a broader range of NFB latency values.

Reassuringly, the S-shaped profiles observed in the results for burst magnitude (the first column) for FB0-FBMock and FB0-FB500 pairs replicate the profiles present in the incidence rate curves (the second column) and the linear

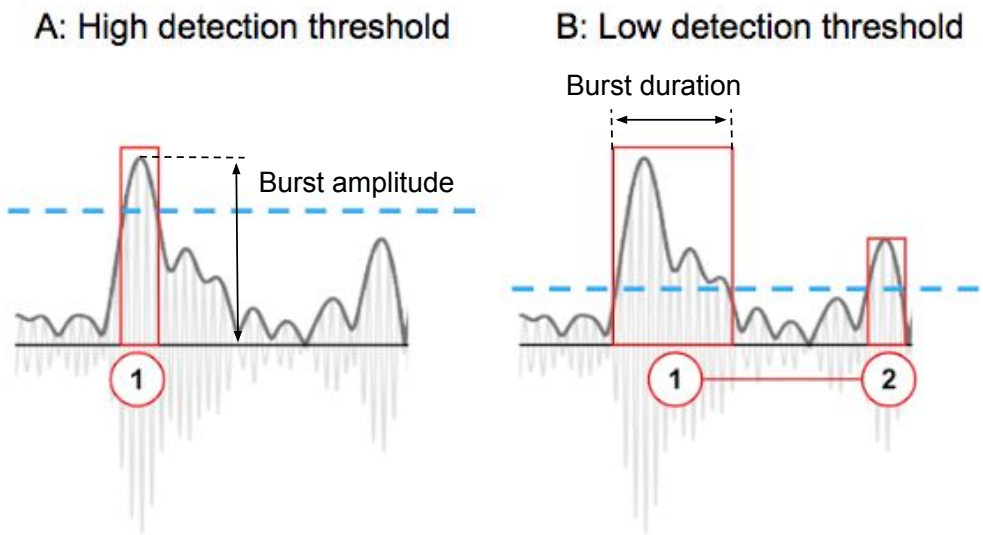

Figure 7: Detection of alpha bursts with different threshold values. Burst amplitude and duration characteristics. The curve represents alpha envelope. A: A single, narrow burst is selected with a high threshold B: The selected burst widens and an additional burst is detected with a lower threshold.

trends observed for the other pairs are also very similar when magnitude and incidence rate data are compared. Finally, both magnitude and the incidence rate curves differ when FB0 and FB500 conditions are compared, and an S-shaped differential profile is revealed ($p = 0.0237$, FDR corrected). As evident from Figure 8 B that shows superimposed parametric profiles for the statistically significant difference, FB0 vs. FB500 and FB0 vs. FBMock shape difference contains a steep slope and a prominent decline at the end of the training contributed by FB0 condition.

The threshold value used for detection of alpha spindles could significantly affect the results described above. To explore the robustness of our findings, we repeated the above analyses for a range of threshold factor values $\mu \in [1,\ 3]$. These results are summarized in Figure 9 where the FDR-corrected p-values obtained with AN-test comparing the corresponding pairs of conditions are color-coded. One can observe statistically significant variations in the learning curves for the incidence rate parameter for the majority of the explored thresholds when comparing true NFB conditions with mock NFB. Also, for a limited range of intermediate threshold values, significant changes are present in the shapes of the incidence rate learning curves for comparison of FB0 and FB500 conditions.

For a small range of thresholds that corresponds to low values of μ we consistently observe significant changes in burst duration and amplitude for the three true feedback conditions with respect to FBMock. These differences are stronger for FB500 condition where they are present for a broader range of threshold values. Interestingly, one can see a somewhat complementary pictures in comparisons between the three feedback conditions and mock feedback. For the subset of low threshold values we have observed differences in training dynamics for the amplitude and duration of alpha bursts whereas no difference is present in the incidence rate of alpha spindles. Yet, for the other(by far larger) contiguous subset of threshold values a difference is present in the incidence rate but not in burst amplitude and duration parameters.

Sustained changes in the structure of alpha activity

We also analyzed the sustained changes in the parameters of alpha spindles caused by NFB training. The results are summarized in panels B)-D) of Figure 6. In panel B) one can see an increase in spindles incidence rate in the post-training baseline as compared to the pre-training data: this effect is significant for FB0 and FB250 conditions. By visual inspection, the effect is stronger for FB0 and the CI of the difference is shifted to the right as compared to FB250 condition. One can also see a small but consistent and significant ($p < 0.01$) increase of burst amplitude for FB0 but not the other conditions. Therefore we can conclude that the incidence rate of alpha bursts hallmarks successful learning and can be used to monitor learning progress during the training as well as to judge the post-effects of NFB intervention. Interestingly and importantly, feedback presentation latency affects the extent to which NFB induced changes persist after the training.

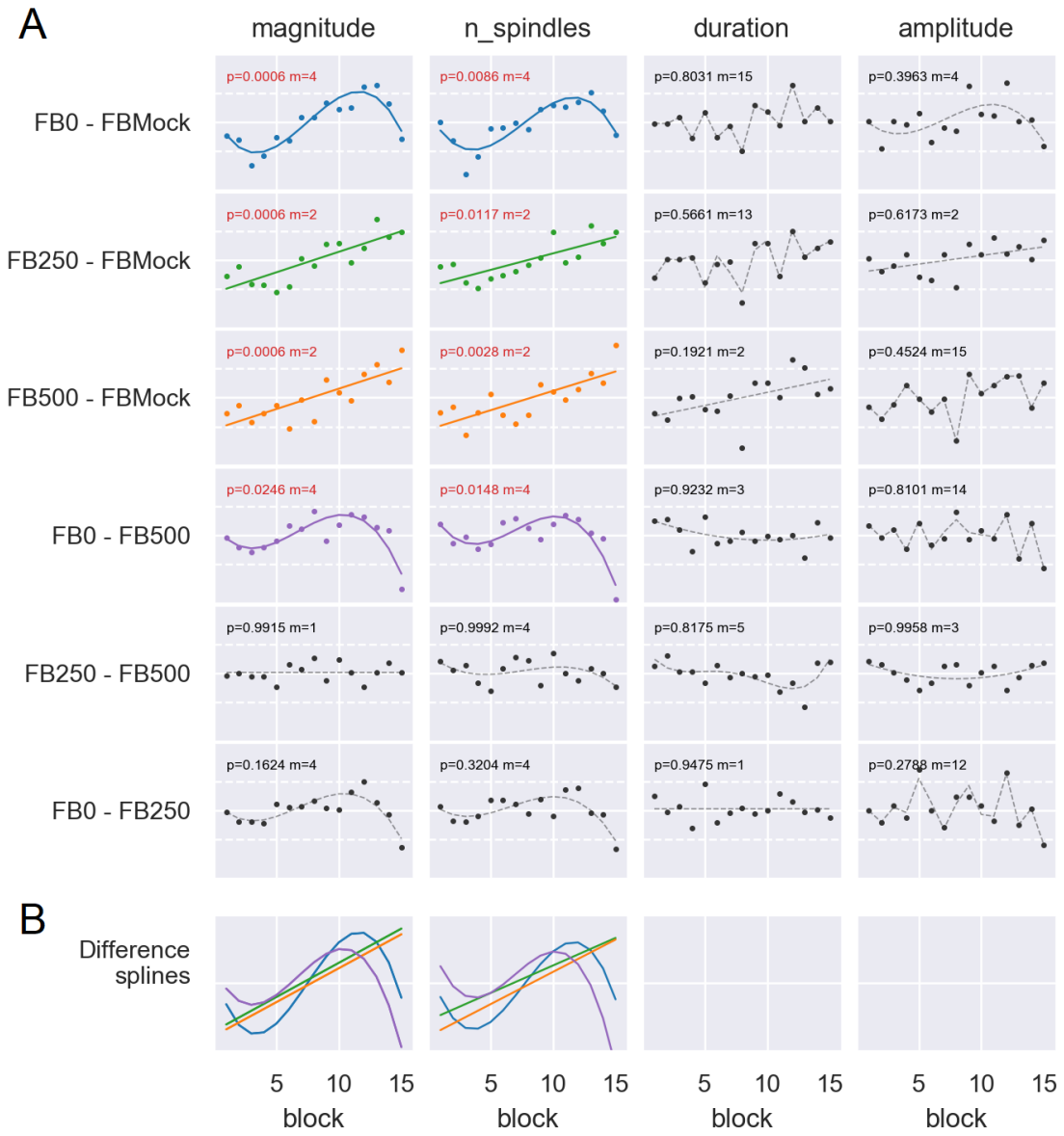

Figure 8: A) Pairwise t-statistics and AN-test results comparing dynamics of changes in the three morphological characteristics of alpha activity between all pairs of conditions for threshold factor $\mu = 2.5$. p-values are FDR corrected. To facilitate comparison we have also included magnitude dynamics as the left-most column B) Superimposed parametric representations of the statistically significant difference between the compared learning curves. The difference exists only in magnitude and the incidence rate parameters.

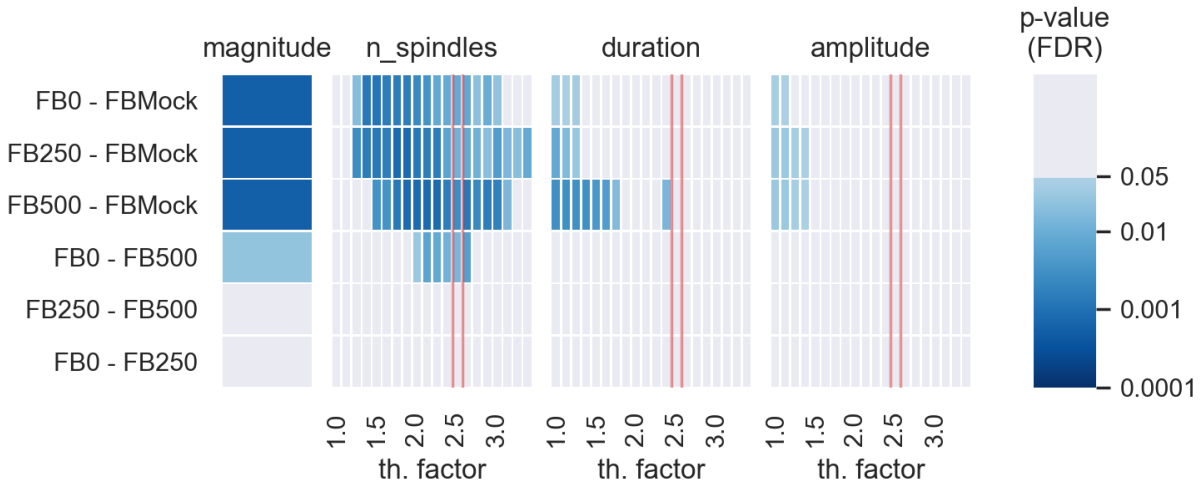

Figure 9: FDR corrected p-values for the pairwise AN-test exploring the effect of feedback latency on different morphological characteristics of the P4 alpha rhythm. Separate tests are performed for each threshold factor μ in a range from 1 to 3. The color indicates statistical significance based on $\alpha = 0.05$ significance level. Red lines indicates results for optimal threshold factor $\mu = 2.5$ corresponding to the minimal mutual information between the three morphological characteristics of the alpha-band activity

Discussion

In this study, subjects were aided with NFB so that they could increase their parietal alpha activity. We implemented an experimental paradigm where NFB latency was precisely controlled and manipulated programmatically. The minimal latency that we could achieve with our hardware and software setup was the end-to-end delay of 244 ms, of which 100 ms corresponded to the causal estimation of the narrow-band EEG envelope [56]. We either kept this latency fixed or artificially imposed an extra delay. Additionally, a mock NFB condition was tested. The four experimental conditions (0, 250 and 500-ms added delays, and mock NFB) were run in separate groups of subjects.

During experimental planning, we reasoned that 10 subjects needed to be tested per group, making a total of 40 subjects. This is an appropriate sample for an exploratory/proof-of concept study, which is also consistent with the literature. Indeed, 10 subjects per group with test power of 0.8 would allow us to detect correlation of $\rho = 0.7$ between a parameter of interest and the training block number, which corresponds to correlation coefficient values observed in our previous study [41]. To explore more subtle effects, we took measures to increase the statistical power of our testing procedure. We employed a SNR based stratification procedure and used data normalization step to reduce inter-subject variability. Furthermore, we used the adaptive Neyman test and compared the learning curves which exploits their potential smoothness. When comparing baseline activity levels we used a paired test. Data from 5 subjects had to be removed because of the problems with EEG recordings (see Methods), which slightly decreased our sample compared to the original plan.

Our detailed study of the latency effects extends the previous work where cortical alpha rhythm served as the source of NFB [36], [1], [12], [19], [21], [61], [41]. In agreement with these previous studies, our subjects were able to increase the average magnitude of their alpha activity during 30 minutes of NFB training, and for the shortest NFB latency this increase was sustained after the training. By contrast, only a small increase in alpha activity was observed with mock NFB.

Consistent with our previous study [41], we observed clear changes in the incidence rate of alpha-activity bursts: as participants trained with NFB, these neural events became more frequent. Other changes in the structure of alpha-band activity, such as amplitude and duration of alpha bursts, were significantly less pronounced.

Interestingly, this result replicates our earlier findings [41] that showed, under different experimental settings, that NFB affects the incidence rate of alpha-spindles rather than influencing their shape. Thus, alpha spindles could be considered as discrete events whose probability changes as the result of NFB training. Relevant observations have been made regarding the beta-band transient events whose incidence rate, but not duration or amplitude predict motor performance across a range of species[54]. Thus, mean power in a particular spectral band – the parameter that has been traditionally used as a target parameter for NFB – crucially depends on the rate of occurrence of the discrete harmonic

events. Therefore, we envision a NFB paradigm where these discrete short-lived events are specifically targeted by operant conditioning which in turn requires timely feedback presentation.

The goal of NFB training can be defined as the achievement of sustained changes in certain neural patterns. Therefore, the finding is important that only the lowest-latency NFB resulted in a sustained effect in our experiments. For this condition, average alpha amplitude was elevated, as evident from the comparison of baseline EEG recorded prior to NFB training with the EEG recorded after the training was completed (Figure 6.A). Incidence rate of alpha spindles was the major parameter that accounted for this change in baseline activity. Curiously, spindle rate increased not only for the shortest latency but also weakly for the condition where 250 ms were added to the base latency (Figure 6.B). In addition to the major effect of spindle rate, we observed a small but consistent and statistically significant change in the amplitude of alpha-spindles that occurred only for the shortest latency (Figure 6.C).

Several insights regarding the role of NFB latency can be gained from Figure 4. For the lowest latency, the initial rise in alpha activity was the steepest compared to the other conditions. Following the rise, alpha activity stabilized earlier and at a higher level when the latency was the shortest. Curiously, for the lowest latency, alpha activity declined over the last three training blocks. We used the adaptive Neyman test (AN-test) [15] useful to quantify this complex behavior. This test revealed an S-shaped profile for training with the lowest NFB latency whereas the dynamics for the longer latencies were best described as linear trends that clearly differed from the trend for mock NFB. These results can be appreciated in Figure 5 that shows the time course of these changes and the splines fitted to t-statistics profiles x_k, $k = 1, \ldots, 15$ (see Appendix: Comparing learning curves for details). Spindle incidence rate practically mirrored the time course of average alpha amplitude. By contrast, the curves for spindle amplitude and duration were not significantly different from those observed for mock NFB. The contribution of spindle rate was quite robust as it persisted for a broad range of threshold values that defined spindle events.

Having established that NFB latency had a strong effect on spindle rate and little effect on the other parameters of alpha activity, we need to find an explanation for this finding. We suggest that our results could be explained by a reinforcement-learning mechanism, where NFB reinforces a neural pattern that coincides with NFB arrival, that is Hebbian plasticity is involved that strengthens a neural circuit that generates a particular activity pattern. Accordingly, the shorter the latency, the higher is the likelihood that NFB would reinforce the neural pattern that triggered the NFB, whereas a reinforcement that arrives with a lag would have a weaker effect on original neural pattern and the original circuit (i.e. a temporal discounting effect). Only with minimal NFB latency, robust changes in parietal alpha activity could be achieved. In this shortest-delay condition, NFB was initiated by an alpha spindle and arrived when the spindle was still ongoing, which reinforced the spindle and made its occurrence in the future more probable. Since an alpha spindle is a cortical event that has a stable structure (amplitude and duration), such reinforcement mechanism affects primarily the rate of this event but not its shape or duration. With the longer latencies of 250-500 ms, NFB is much less temporally specific and consequently less effective. Indeed, with the longer latency, NFB became less specific to the desired state transition to the oscillatory state simply because of increased likelihood that the original spindle has already completed by the time NFB arrives. Notably, participants in our experiments were asked to avoid any conscious strategy for modulating alpha activity. Under these conditions, learning was automatic and dependent on the Hebbian mechanism described above.

Overall, our findings suggest that NFB latency is a crucial parameter that needs to be minimized to achieve desired changes in the fine characteristics of EEG activity. While we experimented with relatively long NFB delays in this study, future work should examine shorter delays, particularly those on the order of 50 ms and lower. Such a low latency would enhance the sense of agency [14] and harness the power of automatic learning [30] by directly and specifically interacting with brain-state transitions. To achieve this desired latency decrease, more efficient signal processing pipelines are needed that use optimized hardware-software communication protocols, as well as more sophisticated signal processing pipelines for the extraction of oscillation parameters from brain activity [56, 34, 52].

Acknowledgements

This work is supported by the Center for Bioelectric Interfaces NRU HSE, RF Government grant, ag. No.14.641.31.0003.

Appendix: Comparing learning curves

For every pair of FB groups, we compared learning curves between the two conditions and tested the null hypothesis (H0) about similarity of the learning curves. For such hypothesis testing, we used the adaptive Neyman test (AN-test) described in [15]. In contrast to the simple 2-sample T-test, AN-test takes into account the temporal connectivity between curve points. Also, in contrast to linear regression models, AN-test is not restricted to the linear learning

curve prior and allows curves and the mean difference between the curves to be nonlinear. The steps of this test are the following:

1. For each pair of conditions $\{i, j\}$ and for each block number $k = 1..15$ compute T-statistic x_k to estimate the difference between average learning curves:

$$x_k = \frac{\bar{y}_i(t) - \bar{y}_j(t)}{\sqrt{n_i^{-1}\hat{\sigma}_i^2(t) + n_j^{-1}\hat{\sigma}_j^2(t)}} \tag{1}$$

   , where $\bar{y}_i(k)$, $\hat{\sigma}_i(k)$ and $\bar{y}_j(k)$, $\hat{\sigma}_j(k)$, are the sample mean and sample standard deviation for the k-th training block in the i-th and j-th conditions, see also formula (13) in the original paper [15].

2. Represent vector $\mathbf{x} = (x_1, ..., x_{15})$ as a linear combination of predefined basis vectors $\mathbf{b}_n$ (n=1..15) that form transform matrix $\mathbf{B}$. The corresponded coefficients of such decomposition can be obtained as $\mathbf{x}^* = \mathbf{B}\mathbf{x} = (x_1^*, ..., x_{15}^*)$. In the original paper this decomposition is obtained by Fourier transform. Here we used basis vectors $\mathbf{b}_n$ that corresponded to the discrete version of Legendre polynomials. This way the basis vectors describe the following temporal features: $\mathbf{b_1}$ - *constant level*, $\mathbf{b_2}$ - *linear trend*, $\mathbf{b_3}$ - *U-shaped curve*, $\mathbf{b_4}$ - *S-shaped curve*, etc. We expected that learning curves have more natural representation as the weighted sum of such temporal features rather than that formed with Fourier basis.

3. For the first m coefficients $x_1^*, ...x_m^*$ ($m = 1..15$) estimate final statistics (see formula (6) [15]). Find m^* for which the statistic reaches maximal value T_{AN}^*. If T_{AN}^* is too large than H0 can be rejected.

To determine the p-value we used finite sample distribution of T_{AN}^* based on 200 thousand Monte-Carlo simulations. This distribution was obtained for each degree of freedom for the T-statistic in step 1. Note that the number of degrees of freedom is defined here as $df = n_1 + n_2 - 2$ where n_1 and n_2 is number of subjects in the first and second conditions in the pair. Additionally, we used value m^* from step 3 to recover smooth approximation $\hat{\mathbf{x}}$ of learning curves difference by using the inverse transform $\hat{\mathbf{x}} = \mathbf{B}^{-1}\hat{\mathbf{x}}^*$, where $\hat{\mathbf{x}}^* = (x_1^*, x_2^*..., x_{m^*}^*, 0, ..., 0)$ is a vector of length 15 which contains only first m^* non-zero coefficients.

References

[1] S. Agnoli, M. Zanon, S. Mastria, A. Avenanti, and G. E. Corazza. Enhancing creative cognition with a rapid right-parietal neurofeedback procedure. *Neuropsychologia*, 118:99–106, 2018.

[2] O. Alkoby, A. Abu-Rmileh, O. Shriki, and D. Todder. Can we predict who will respond to neurofeedback? a review of the inefficacy problem and existing predictors for successful EEG neurofeedback learning. *Neuroscience*, 378:155–164, 2018.

[3] M. Arns, S. De Ridder, U. Strehl, M. Breteler, and A. Coenen. Efficacy of neurofeedback treatment in adhd: the effects on inattention, impulsivity and hyperactivity: a meta-analysis. *Clinical EEG and neuroscience*, 40(3):180–189, 2009.

[4] Y. Bagherzadeh, D. Baldauf, D. Pantazis, and R. Desimone. Alpha synchrony and the neurofeedback control of spatial attention. *Neuron*, 105(3):577–587, 2020.

[5] M. J. Batty, S. Bonnington, B.-K. Tang, M. B. Hawken, and J. H. Gruzelier. Relaxation strategies and enhancement of hypnotic susceptibility: EEG neurofeedback, progressive muscle relaxation and self-hypnosis. *Brain research bulletin*, 71(1-3):83–90, 2006.

[6] D. Beamish, S. Bhatti, J. Wu, and Z. Jing. Performance limitations from delay in human and mechanical motor control. *Biological cybernetics*, 99(1):43–61, 2008.

[7] G. Buzsáki. *Rhythms of the brain*. Oxford Univ. Press, 2011.

[8] R. L. Cannon. Parietal foci for attention deficit/hyperactivity disorder: Targets for loreta neurofeedback with outcomes. *Biofeedback*, 42(2):47–57, 2014.

[9] J. Y. Chen and J. E. Thropp. Review of low frame rate effects on human performance. *IEEE Transactions on Systems, Man, and Cybernetics-Part A: Systems and Humans*, 37(6):1063–1076, 2007.

[10] A. Cortoos, E. De Valck, M. Arns, M. H. Breteler, and R. Cluydts. An exploratory study on the effects of tele-neurofeedback and tele-biofeedback on objective and subjective sleep in patients with primary insomnia. *Applied psychophysiology and biofeedback*, 35(2):125–134, 2010.

[11] P. Dehghanpour, F. Farokhi, and R. Rostami. Improvement of working memory performance by parietal upper alpha neurofeedback training. *International Journal of Smart Electrical Engineering*, 7(02):77–81, 2018.

[12] T. Egner, E. Strawson, and J. H. Gruzelier. EEG signature and phenomenology of alpha/theta neurofeedback training versus mock feedback. *Applied psychophysiology and biofeedback*, 27(4):261, 2002.

[13] C. Escolano, M. Navarro-Gil, J. Garcia-Campayo, M. Congedo, D. De Ridder, and J. Minguez. A controlled study on the cognitive effect of alpha neurofeedback training in patients with major depressive disorder. *Frontiers in behavioral neuroscience*, 8:296, 2014.

[14] N. Evans, S. Gale, A. Schurger, and O. Blanke. Visual feedback dominates the sense of agency for brain-machine actions. *PloS one*, 10(6):e0130019, 2015.

[15] J. Fan and S.-K. Lin. Test of significance when data are curves. *Journal of the American Statistical Association*, 93(443):1007–1021, 1998.

[16] C. Farrer, G. Valentin, and J. Hupé. The time windows of the sense of agency. *Consciousness and cognition*, 22(4):1431–1441, 2013.

[17] J. Greenspoon and S. Foreman. Effect of delay of knowledge of results on learning a motor task. *Journal of Experimental Psychology*, 51(3):226, 1956.

[18] J. Gruzelier. A theory of alpha/theta neurofeedback, creative performance enhancement, long distance functional connectivity and psychological integration. *Cognitive processing*, 10(1):101–109, 2009.

[19] J. H. Gruzelier. EEG-neurofeedback for optimising performance. i: a review of cognitive and affective outcome in healthy participants. *Neuroscience & Biobehavioral Reviews*, 44:124–141, 2014.

[20] J. H. Gruzelier. EEG-neurofeedback for optimising performance. iii: a review of methodological and theoretical considerations. *Neuroscience & Biobehavioral Reviews*, 44:159–182, 2014.

[21] S. Hanslmayr, P. Sauseng, M. Doppelmayr, M. Schabus, and W. Klimesch. Increasing individual upper alpha power by neurofeedback improves cognitive performance in human subjects. *Applied psychophysiology and biofeedback*, 30(1):1–10, 2005.

[22] G. Huang, J. Liu, L. Li, L. Zhang, Y. Zeng, L. Ren, S. Ye, and Z. Zhang. A novel training-free externally-regulated neurofeedback (er-nf) system using phase-guided visual stimulation for alpha modulation. *NeuroImage*, 189:688–699, 2019.

[23] R. B. Ivry and R. M. Spencer. The neural representation of time. *Current opinion in neurobiology*, 14(2):225–232, 2004.

[24] K. C. Kadosh and G. Staunton. A systematic review of the psychological factors that influence neurofeedback learning outcomes. *NeuroImage*, 185:545–555, 2019.

[25] J. Kamiya. Conscious control of brain waves. *PsycEXTRA Dataset*, 1968.

[26] J. Kamiya. Operant control of the EEG alpha rhythm and some of its reported effects on consciousness. *Alerted states of consciousness*, 489, 1969.

[27] S. W. Keele and M. I. Posner. Processing of visual feedback in rapid movements. *Journal of experimental psychology*, 77(1):155, 1968.

[28] S. E. Kober, G. Wood, J. Kurzmann, E. V. Friedrich, M. Stangl, T. Wippel, A. Väljamäe, and C. Neuper. Near-infrared spectroscopy based neurofeedback training increases specific motor imagery related cortical activation compared to sham feedback. *Biological psychology*, 95:21–30, 2014.

[29] C. Kothe. Lab streaming layer (lsl). `https://github.com/sccn/labstreaminglayer`, 2015.

[30] J. M. Lacroix. Mechanisms of biofeedback control. In *Consciousness and Self-regulation*, pages 137–162. Springer, 1986.

[31] N. Lofthouse, R. Hendren, E. Hurt, L. E. Arnold, and E. Butter. A review of complementary and alternative treatments for autism spectrum disorders. *Autism research and treatment*, 2012, 2012.

[32] J. F. Lubar, M. Congedo, and J. H. Askew. Low-resolution electromagnetic tomography (loreta) of cerebral activity in chronic depressive disorder. *International Journal of Psychophysiology*, 49(3):175–185, 2003.

[33] N. MacDonald and N. MacDonald. *Biological delay systems: linear stability theory*. Cambridge University Press, 2008.

[34] J. R. Mcintosh and P. Sajda. Estimation of phase in EEG rhythms for real-time applications. *Journal of neural engineering*, 2020.

[35] M. Meehan, S. Razzaque, M. C. Whitton, and F. P. Brooks. Effect of latency on presence in stressful virtual environments. In *IEEE Virtual Reality, 2003. Proceedings.*, pages 141–148. IEEE, 2003.

[36] D. P. Nowlis and J. Kamiya. The control of electroencephalographic alpha rhythms through auditory feedback and the associated mental activity. *Psychophysiology*, 6(4):476–484, 1970.

[37] E. F. Oblak, J. A. Lewis-Peacock, and J. S. Sulzer. Self-regulation strategy, feedback timing and hemodynamic properties modulate learning in a simulated fmri neurofeedback environment. *PLoS computational biology*, 13(7):e1005681, 2017.

[38] Y. O. Okazaki, J. M. Horschig, L. Luther, R. Oostenveld, I. Murakami, and O. Jensen. Real-time meg neurofeedback training of posterior alpha activity modulates subsequent visual detection performance. *Neuroimage*, 107:323–332, 2015.

[39] M. Ordikhani-Seyedlar and M. A. Lebedev. Controlling attention with neurofeedback. In *The Physics of the Mind and Brain Disorders*, pages 545–572. Springer, 2017.

[40] M. Ordikhani-Seyedlar and M. A. Lebedev. Augmenting attention with brain–computer interfaces. *Brain–Computer Interfaces Handbook*, page 549–560, 2018.

[41] A. Ossadtchi, T. Shamaeva, E. Okorokova, V. Moiseeva, and M. A. Lebedev. Neurofeedback learning modifies the incidence rate of alpha spindles, but not their duration and amplitude. *Scientific reports*, 7(1):3772, 2017.

[42] F. Peeters, J. Ronner, L. Bodar, J. van Os, and R. Lousberg. Validation of a neurofeedback paradigm: manipulating frontal EEG alpha-activity and its impact on mood. *International Journal of Psychophysiology*, 93(1):116–120, 2014.

[43] S. W. Phneah and H. Nisar. EEG-based alpha neurofeedback training for mood enhancement. *Australasian physical & engineering sciences in medicine*, 40(2):325–336, 2017.

[44] M. Richelle, H. Lejeune, D. Defays, P. Greenwood, F. Macar, and H. Mantanus. *Time in animal behaviour*. Elsevier, 2013.

[45] A. Ridder and Z. Botev. Variance reduction. *Wiley StatsRef: Statistics Reference Online*, pages 1–6, 2017.

[46] T. Ros, S. Enriquez-Geppert, V. Zotev, K. Young, G. Wood, S. Whitfield-Gabrieli, F. Wan, F. Vialatte, D. Van De Ville, D. Todder, et al. Consensus on the reporting and experimental design of clinical and cognitive-behavioural neurofeedback studies (cred-nf checklist). 2019.

[47] S. Sampath. *Sampling theory and methods*. CRC press, 2001.

[48] C.-E. Särndal, B. Swensson, and J. Wretman. *Model assisted survey sampling*. Springer Science & Business Media, 2003.

[49] W. N. Schoenfeld. *The theory of reinforcement schedules*. Appleton-Century-Crofts NewYork, 1970.

[50] A. Sengül, F. Rivest, M. Van Elk, O. Blanke, and H. Bleuler. Visual and force feedback time-delays change telepresence: Quantitative evidence from crossmodal congruecy task. In *2013 World Haptics Conference (WHC)*, pages 577–582. Ieee, 2013.

[51] M. Shahrokh Esfahani and E. R. Dougherty. Effect of separate sampling on classification accuracy. *Bioinformatics*, 30(2):242–250, 2013.

[52] A. Shakeel, T. Tanaka, and K. Kitajo. Time-series prediction of the oscillatory phase of EEG signals using the least mean square algorithm-based AR model. *Applied Sciences*, 10:3616, 05 2020.

[53] L. H. Sherlin, M. Arns, J. Lubar, H. Heinrich, C. Kerson, U. Strehl, and M. B. Sterman. Neurofeedback and basic learning theory: implications for research and practice. *Journal of Neurotherapy*, 15(4):292–304, 2011.

[54] H. Shin, R. Law, S. Tsutsui, C. I. Moore, and S. R. Jones. The rate of transient beta frequency events predicts behavior across tasks and species. *Elife*, 6:e29086, 2017.

[55] R. Sitaram, T. Ros, L. Stoeckel, S. Haller, F. Scharnowski, J. Lewis-Peacock, N. Weiskopf, M. L. Blefari, M. Rana, E. Oblak, et al. Closed-loop brain training: the science of neurofeedback. *Nature Reviews Neuroscience*, 18(2):86, 2017.

[56] N. Smetanin, A. Belinskaya, M. Lebedev, and A. Ossadtchi. Digital filters for low-latency quantification of brain rhythms in real-time. *Journal of Neural Engineering*, 2020.

[57] N. Smetanin, K. Volkova, S. Zabodaev, M. Lebedev, and A. Ossadtchi. Nfblab-a versatile software for neurofeedback and brain-computer interface research. *Frontiers in neuroinformatics*, 12:100, 2018.

[58] S. Staufenbiel, A.-M. Brouwer, A. Keizer, and N. Van Wouwe. Effect of beta and gamma neurofeedback on memory and intelligence in the elderly. *Biological psychology*, 95:74–85, 2014.

[59] J. Sulzer, S. Haller, F. Scharnowski, N. Weiskopf, N. Birbaumer, M. L. Blefari, A. B. Bruehl, L. G. Cohen, R. C. DeCharms, R. Gassert, et al. Real-time fmri neurofeedback: progress and challenges. *Neuroimage*, 76:386–399, 2013.

[60] R. T. Thibault, M. Lifshitz, and A. Raz. The self-regulating brain and neurofeedback: experimental science and clinical promise. *cortex*, 74:247–261, 2016.

[61] D. Vernon, T. Dempster, O. Bazanova, N. Rutterford, M. Pasqualini, and S. Andersen. Alpha neurofeedback training for performance enhancement: reviewing the methodology. *Journal of neurotherapy*, 13(4):214–227, 2009.

[62] D. Vernon, T. Egner, N. Cooper, T. Compton, C. Neilands, A. Sheri, and J. Gruzelier. The effect of training distinct neurofeedback protocols on aspects of cognitive performance. *International journal of psychophysiology*, 47(1):75–85, 2003.

[63] D. Vernon, A. Frick, and J. Gruzelier. Neurofeedback as a treatment for adhd: A methodological review with implications for future research. *Journal of Neurotherapy*, 8(2):53–82, 2004.

[64] F. Wan, W. Nan, M. I. Vai, and A. Rosa. Resting alpha activity predicts learning ability in alpha neurofeedback. *Frontiers in human neuroscience*, 8:500, 2014.

[65] T. Watanabe, Y. Sasaki, K. Shibata, and M. Kawato. Advances in fmri real-time neurofeedback. *Trends in cognitive sciences*, 21(12):997–1010, 2017.

[66] J. Wu. *Introduction to neural dynamics and signal transmission delay*, volume 6. Walter de Gruyter, 2011.

[67] S. Xiong, C. Cheng, X. Wu, X. Guo, L. Yao, and J. Zhang. Working memory training using EEG neurofeedback in normal young adults. *Bio-medical materials and engineering*, 24(6):3637–3644, 2014.

[68] H. G. Yamin, T. Gazit, N. Tchemodanov, G. Raz, G. Jackont, F. Charles, I. Fried, T. Hendler, and M. Cavazza. Depth electrode neurofeedback with a virtual reality interface. *Brain-Computer Interfaces*, 4(4):201–213, 2017.

[69] B. Zoefel, R. J. Huster, and C. S. Herrmann. Neurofeedback training of the upper alpha frequency band in EEG improves cognitive performance. *Neuroimage*, 54(2):1427–1431, 2011.

[70] A. Zuberer, D. Brandeis, and R. Drechsler. Are treatment effects of neurofeedback training in children with adhd related to the successful regulation of brain activity? A review on the learning of regulation of brain activity and a contribution to the discussion on specificity. *Frontiers in human neuroscience*, 9:135, 2015.